

The Pursuit of Engineering the Ideal Heart Valve Replacement or Repair

***Ex Vivo* Methods for Informing Computational Models of the Mitral Valve**

CHARLES H. BLOODWORTH IV,¹ ERIC L. PIERCE,¹ THOMAS F. EASLEY,¹ ANDREW DRACH,²
AMIR H. KHALIGHI,² MILAN TOMA,¹ MORTEN O. JENSEN,¹ MICHAEL S. SACKS,² and AJIT P. YOGANATHAN¹

¹Cardiovascular Fluid Mechanics Laboratory, Wallace H. Coulter Department of Biomedical Engineering, Georgia Institute of Technology and Emory University, 387 Technology Circle NW, Suite 200, Atlanta, GA 30313, USA; and ²Center for Cardiovascular Simulation, Institute for Computational Engineering and Sciences, The University of Texas at Austin, 201 E. 24th Street, Austin, TX 78712, USA

(Received 8 February 2016; accepted 12 September 2016; published online 3 October 2016)

Associate Editor Lakshmi Prasad Dasi oversaw the review of this article.

Abstract—Computational modeling of the mitral valve (MV) has potential applications for determining optimal MV repair techniques and risk of recurrent mitral regurgitation. Two key concerns for informing these models are (1) sensitivity of model performance to the accuracy of the input geometry, and, (2) acquisition of comprehensive data sets against which the simulation can be validated across clinically relevant geometries. Addressing the first concern, *ex vivo* micro-computed tomography (microCT) was used to image MVs at high resolution (~40 micron voxel size). Because MVs distorted substantially during static imaging, glutaraldehyde fixation was used prior to microCT. After fixation, MV leaflet distortions were significantly smaller ($p < 0.005$), and detail of the chordal tree was appreciably greater. Addressing the second concern, a left heart simulator was designed to reproduce MV geometric perturbations seen *in vivo* in functional mitral regurgitation and after subsequent repair, and maintain compatibility with microCT. By permuting individual excised ovine MVs ($n = 5$) through each state (healthy, diseased and repaired), and imaging with microCT in each state, a comprehensive data set was produced. Using this data set, work is ongoing to construct and validate high-fidelity MV biomechanical models. These models will seek to link MV function across clinically relevant states.

Keywords—Mitral regurgitation, Mitral repair, Simulation, Cardiovascular, Imaging, Micro-computed tomography.

INTRODUCTION

Valvular heart disease (VHD) is estimated to affect 2.5% of the population in industrialized countries, and the prevalence of VHD increases drastically in elderly populations.¹⁴ Functional Mitral Regurgitation (MR) is a form of VHD where remodeling and displacement of the papillary muscles (PMs) and mitral annulus cause MV insufficiency. A form of functional MR, known as Ischemic Mitral Regurgitation (IMR), is caused by adverse remodeling of the left ventricle (LV). Though the geometric distortions vary widely, PM displacement, annular dilatation, and leaflet tethering are widely accepted as the causes of MR with inferior myocardial infarct.^{2,30} This may result in pulmonary hypertension, dyspnea, and atrial dysfunction, among other complications.²

To treat symptomatic IMR, the MV structures are either repaired, or the MV is replaced altogether. Due to lower perioperative mortality, and better long-term survival rates, repair is a popular option for treating IMR.^{3,6,9} However, long-term recurrence of moderate to severe MR is still prevalent in MV repair patients.^{1,18} Although the exact mechanism of MR recurrence can vary, adverse leaflet/chordal loading, ventricular remodeling, and leaflet stress concentrations are all implicated as causes.^{13,18} Given these mixed outcomes, and the ever-expanding variety of repair devices and procedures,⁸ the best treatment option for each individual patient is often unclear.^{2,9} The key to optimal repair selection for an individual lies in understanding the function of the MV on a

Address correspondence to Ajit P. Yoganathan, Cardiovascular Fluid Mechanics Laboratory, Wallace H. Coulter Department of Biomedical Engineering, Georgia Institute of Technology and Emory University, 387 Technology Circle NW, Suite 200, Atlanta, GA 30313, USA. Electronic mail: ajit.yoganathan@bme.gatech.edu

patient-specific basis, both in its diseased state, and in response to different repair options. One approach, which is particularly well suited to studying functional change of the MV and load redistribution within the MV, is computational modeling. Models of the MV can potentially inform repair efficacy and durability in general or on a patient-specific basis.

Pioneering computational models of MV function utilized simplified MV geometries and material properties, including idealized 1D chordal elements and simplified, planar leaflet surfaces.^{17,26,34} In the past several years, significant improvements have been made in MV model fidelity, largely due to advances in imaging technology, segmentation methods, and computational power.²⁶ Models now aim to simulate MV function with more complex, patient/subject-specific MV geometries in which the finer details and features of the MV are captured.^{19,26,29} Clinical imaging (3D gated ultrasound, multi-slice computed tomography and magnetic resonance imaging) has been the widely used method of choice for obtaining the patient geometries to create these computational models.²⁶ While in the best of cases, these imaging techniques can capture the leaflet geometry and sub-valvular apparatus of a patient's MV, the quality is not often adequate and can be highly variable.³⁵ Furthermore, the patients are commonly only imaged pre- and post-operatively, so only diseased and repaired MV function is available.

The sensitivity of simulation results to the accuracy of the starting geometries has been recently emphasized,^{19,33} making imaging a critical component of the process. In order to utilize computational models to understand patient-specific loading and functional changes in disease and after repair, more reliable methods of capturing and incorporating the finer details of the leaflets and chordal structures are necessary, not only in the healthy case, but also in diseased and surgically repaired cases. In the laboratory setting, *ex vivo* MV simulation and imaging can be leveraged to control the functional state of the MV, and reliably acquire higher resolution 3D images of explanted MVs in a repeated-measures fashion. Using state-of-the-art benchtop imaging modalities, specifically micro-computed tomography (microCT), complex MV structures can be visualized, making the benchtop setting a promising option to tackle this challenge.^{7,29}

To this end, we present a novel benchtop platform which is compatible with microCT imaging, and is capable of simulating, on a single explanted MV, the geometric remodeling observed when the MV becomes diseased (specifically IMR), and when the MV is subsequently repaired. Additionally, we present microCT imaging methodologies, which enable the researcher to acquire high-resolution anatomical 3D images of the

MV, in the diastolic *and* systolic valve configurations, in each of the geometric states (healthy, diseased and repaired). Using this platform, we are able to provide accurate, detailed microCT images of the MV *across* clinically relevant geometries, each in various states of loading. Work is ongoing to directly use these data to construct, develop and validate computational models which seek to link the performance of the MV in its healthy state, in disease, and after surgical repair.

MATERIALS AND METHODS

Ex Vivo Left Heart Simulation Platform

To study the structure and function of each MV, an *ex vivo* left heart simulation platform was employed. MVs were obtained from fresh, never-frozen ovine hearts sourced from Superior Farms (Dixon, CA). MVs with an anterior leaflet length of 18–20 mm and type I or II papillary muscles (PMs) were selected and excised, preserving the annular and sub-valvular geometry. As shown in *Carpentier's Reconstructive Valve Surgery*, these are bulky papillary muscles with either single, or closely clustered PM heads,⁴ which can be securely mounted to the CLHS. Other PM types have widely spread chordal insertion points, and non-continuous PM structure, and cannot be securely attached and correctly oriented within the CLHS. Using a Ford interlocking suture pattern, the mitral annulus was attached to a plate that separates the atrial and ventricular chambers of a previously validated cylindrical left heart simulator (CLHS)²⁵ (Fig. 1a). Referred to here as an

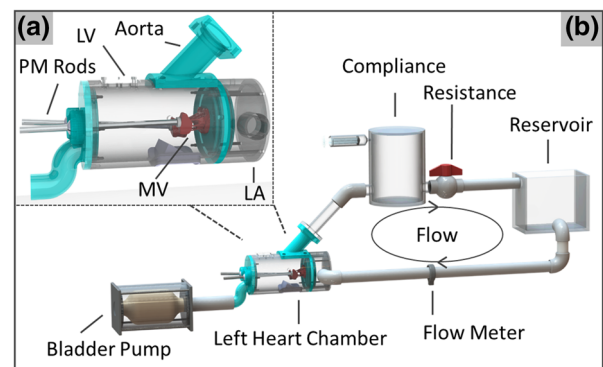


FIGURE 1. (a) The cylindrical left heart simulator (CLHS) features acrylic left atrial (LA) and left ventricular (LV) chambers. An ovine mitral valve (MV) is excised and mounted to the annular plate separating the two compartments. Rods are used to manipulate the positions of the papillary muscles (PMs). (b) The CLHS is inserted into a pulsatile flow loop. A bladder pump is used to drive physiological flows and pressured in the CLHS. Systemic compliance and resistance elements are used to tune the pressure and flow profiles. Pressures and flows are monitored and recorded, along with 3D echo images if the MV.

annulus plate, the plate forms a seal between the left atrium and ventricle, only allowing flow to pass through the annular orifice (described further below). Surrounding the annular orifice is a suture cuff onto which the excised valves are sutured. Care was taken to place the sutures just above the natural leaflet hinge line. The papillary muscles were fixed to movable rods that were used to control their position.

The CLHS was then mounted in a pulsatile flow loop (Fig. 1b). Powered by a bladder pump, the flow loop replicates pressure and flow curves across the MV (peak trans-mitral pressure of 120 mmHg, cardiac output of 5 L per minute, heart rate of 70 beats per minute), causing it to open and close physiologically. Isotonic saline solution was used as the working fluid in this study, because blood viscosity-matched (water-glycerin) solution is not necessary to match bulk pressure and flow, does not significantly affect the geometry of heart valves, and only affects local variation fluid velocity.^{21,36} Furthermore, water glycerin solution can impact tissue valve material properties after prolonged exposure.²¹ Systemic compliance and resistance were adjusted to attain these pressure and flow values. Using echocardiography to clearly visualize the valve coaptation and leaflet shape in real time (iE33 xMATRIX, Philips Healthcare, Andover, MA, USA), PM positions were adjusted to achieve healthy closure (anterior leaflet occupying 2/3 of the A2–P2 diameter, and coaptation length of ~5 mm along the A2–P2 line).²⁵

Simulating Healthy, IMR and Repaired MV Geometries

Geometric remodeling at the annular level is characteristic of IMR.¹¹ To simulate this geometric remodeling, and, subsequently, the changes caused by a flat restrictive annuloplasty repair, a novel adjustable annulus plate was designed (Fig. 2) to fit within the CLHS. This adjustable annulus plate is quasi-static, in that the annular geometry remains stationary during imaging, yet can be readily adjusted between acquisitions to minimize variability. Annular geometric changes were taken from previously published *in vivo* data on MV geometry in healthy and IMR ovine subjects.^{5,30} The dimensions of the repaired annulus were based on the design of the flat, rigid Carpentier-Edwards annuloplasty ring. Table 1 summarizes the geometric parameters that represent the three different geometric MV configurations replicated by the adjustable annulus plate.

To achieve the desired displacements, the adjustable annulus plate employs five repositionable annular segments (blue and red arrows in Figs. 2a and 2b). The five segments are arranged from commissure to commissure along the posterior aspect of the annulus, which experiences the majority of the dilatation in IMR.^{11,30} These adjustable segments travel up and down plastic worm-screws that are seated in the rigid plastic annular plate. The worm-screws rotate in place and are readily adjusted from the outer circumference of the plate. On the anterior aspect of the annulus is a flat, flexible plate which anchors at the anterior horn and can elastically bend out of plane in

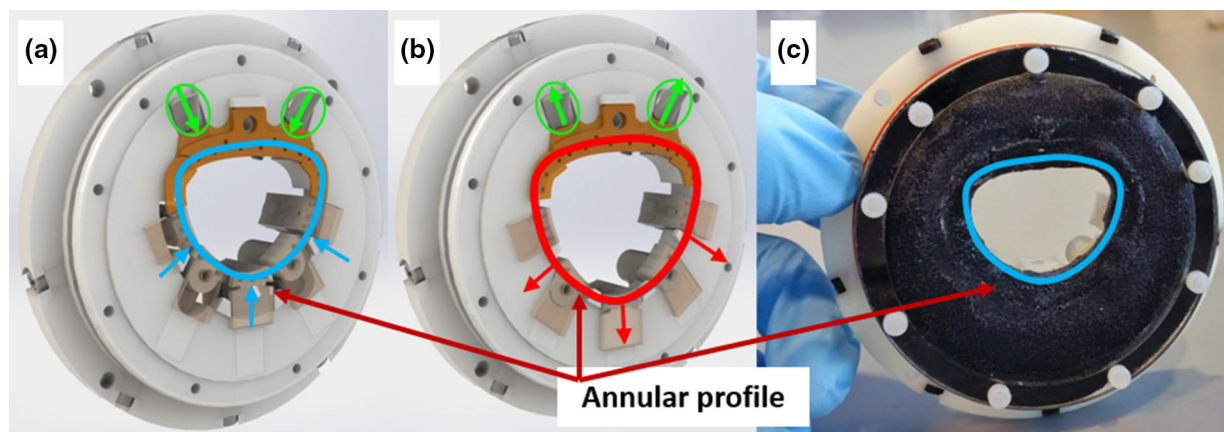


FIGURE 2. Design of the customized annular MV attachment plate to manipulate annular geometry. (a) Computer aided design of the assembly before annular dilatation. Five actuating plastic segments along the posterior aspect of the mitral annulus travel along worm-screw drives seated within the rigid plate. The arrows are overlaid on the segments along the posterior aspect of the annulus. Shown in (b), the position of the segments is adjusted from the outer circumference to pull the segments radially outward to achieve the dilated geometry. Additionally, along the anterior aspect of the annulus, a flexible, laser-cut plastic sheet (orange part directly under green circles) is mounted at the anterior horn. Two wedges, highlighted in green circles, are adjusted to drive the flexible plate apically out of the page at the commissures to achieve a saddle-shaped annular geometry. (c) The final assembly is shown with a black elastic sealing membrane and retainer ring.

TABLE 1. Mitral annular dimensions for healthy, IMR and restrictive annuloplasty MV configurations.

	Healthy	IMR	Restrictive annuloplasty (flat ring)
Anterior–posterior distance (mm)	24	30	24
Inter-commissural distance (mm)	30	33	30
Systolic annular height–commissural width ratio	15%	0% (flat)	0% (flat)

the apical direction at each trigone (orange component in Figs. 2a and 2b). Two plastic wedges, which also travel along worm-screws, are driven under the flexible plate to create the out-of-plane saddle geometry, and retracted to return the annulus back to a planar geometry (green circles in Figs. 2a and 2b). Finally, an elastic, waterproof neoprene membrane was fixed to the annular segments and to the outer circumference of the ventricular face to allow movement of the annulus, and also form a waterproof barrier between the atrium and ventricle (Fig. 2c). All components were custom-fabricated from low-radiopacity plastics and rubbers to minimize attenuation and beam hardening effects during microCT imaging.

Papillary Muscle Manipulation

PM displacement is also characteristic of IMR and ventricular remodeling,²⁵ and was replicated in the CLHS to mimic this remodeling. After establishing healthy MV closure, the PMs were displaced to simulate the LV distension seen with ischemia.^{25,30} Based on *in vivo* studies, the posteromedial PM displacement targets were 4, 6, and 2 mm in the lateral, posterior, and basal directions, respectively. The displacement targets for the anterolateral PM were 2 mm laterally, 1 mm anteriorly, and 1.5 mm apically. To achieve these desired displacements, the PM rods were fixed in water-tight ball-in-socket joints (shown in Fig. 1a), which allow PM adjustment in three dimensions.

Data Acquisition and Imaging Overview

A schematic representing the experimental workflow is shown in Fig. 3. The entire protocol was repeated for five excised ovine MVs ($n = 5$). Before scanning each MV with high-resolution microCT, hemodynamic data (trans-mitral pressure and flow) and real-time 3D echocardiography (3D echo) were recorded for the healthy, diseased and repaired geometries. Whether modeling blood flow through the MV, the valve itself, or both, the hemodynamic data provide the necessary boundary conditions for model construction, as loading on the valve or flow past the valve can be prescribed. Though 3D echo images are of significantly lower resolution than microCT, these

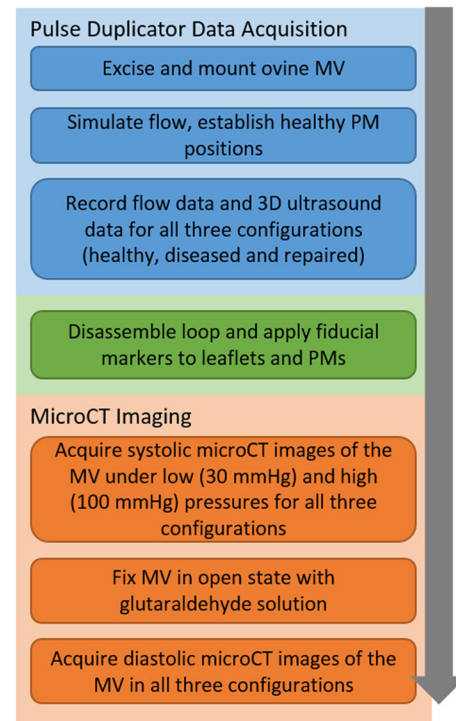


FIGURE 3. Flow chart detailing the order in which data was collected using the methodologies presented, producing comprehensive data sets for model construction and validation.

images provide useful data against which dynamic models can be validated. After these data were collected for each MV configuration, the CLHS was dismounted from the flow loop, drained of saline, and prepared for microCT imaging.

Micro-Computed Tomography Imaging: Preparation and Scan Parameters

Before imaging the MVs with microCT, high-contrast fiducial markers were applied to the surface of the leaflets, the annulus and the PMs (visible in Fig. 4). Described in previously published work by our group, these markers enable the tracking of discrete features, and the calculation of strain between different microCT scans under different loading conditions (Fig. 4b).²⁰ In a modeling setting, this allows the mapping of additional microstructural data to discrete

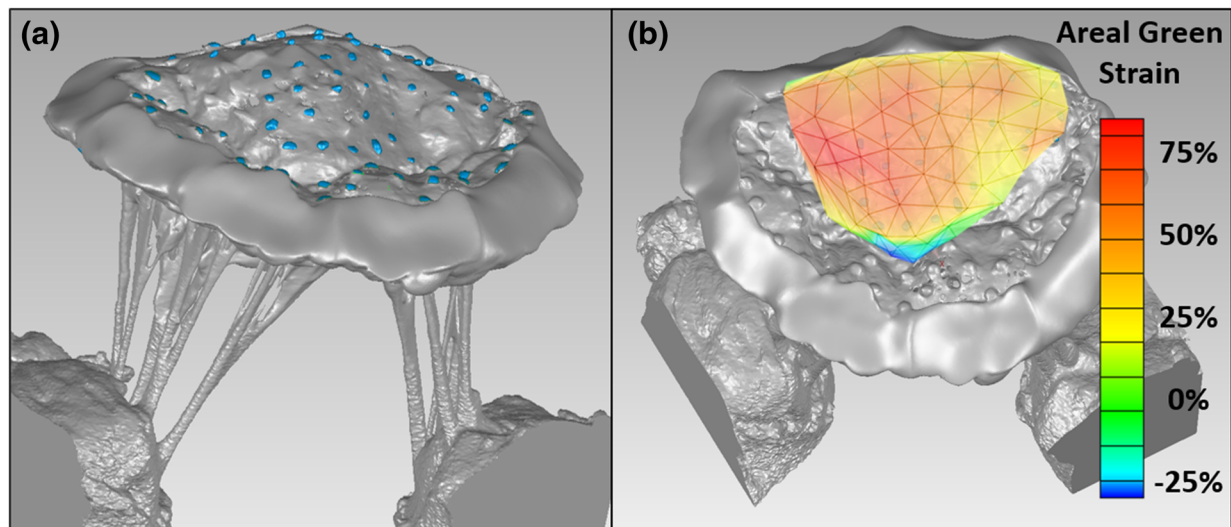


FIGURE 4. (a) Side view of the mitral leaflets and sub-valvular apparatus of a mitral valve loaded at 100 mmHg and imaged by microCT. (b) Using the fiducial marker grid and Eq. (1), anterior leaflet areal green strain was computed with the diastolic microCT scan as the reference configuration, and is overlaid on the systolic MV model. Average strain in the belly region was found to be $47.1 \pm 21.5\%$. Average strain in the coaptation zone was found to be $-12.5 \pm 15.8\%$.

locations on the leaflet surface, as well as precise geometric manipulation of the model. Following marker application, the CLHS was then loaded into a Siemens Inveon microCT scanner (Siemens Corp, Malvern, PA, USA) and scanned with parameters optimized for soft tissue (80 keV, 500 μ A, \sim 40 micron isotropic voxel size). Because the radiopacity of the MV is close to that of water, the MV was imaged in air (the LHS chamber was drained of water) to achieve the necessary level of contrast for subsequent image segmentation.

Micro-Computed Tomography Imaging: Systolic Configuration

High resolution images of each MV under different loading conditions allow for comprehensive validation of computational model performance, not only in the healthy state, but in altered states of disease and repair. By calculating the spatial error between simulation and image, the accuracy of computational models can be evaluated and the model inputs can be effectively tuned. To load and image the MV, pressurized, humidified air was used to close the MV statically for the duration of a 7 min microCT scan. The CLHS was connected to an air pressure source, with an in-line humidifier and regulator, which maintained target LVP \pm 2 mmHg. Each MV was scanned at low and high LVP (30 and 100 mmHg) for each of the three geometric configurations, for a total of six systolic CT scans (representative systolic image shown in Fig. 4).

Micro-Computed Tomography Imaging: Diastolic Configuration

Obtaining a physiologically accurate, high-resolution 3D image of the MV in its diastolic configuration required careful preparation of each MV, as the pliant tissue is prone to warping before imaging. In diastole, blood flows past the MV and into the LV. This causes fluttering, extension and spreading of the MV, which represents the true diastolic structure of the MV, but is incompatible with static imaging. When water was drained from the CLHS for microCT imaging, a folding effect was also observed, which was likely attributable to the cohesive/adhesive forces of the residual water on the surface of the leaflets and chordae tendineae. The surface tension of water caused the thin leaflets to fold on themselves, and the chordae tendineae to clump together, much like a wetted paintbrush (Fig. 5a). When submerged, the leaflets and chordae appeared to spread out and take their natural shape (Fig. 5b).

To capture the diastolic geometry of the MV with microCT, glutaraldehyde was employed as a stiffening agent. Glutaraldehyde is commonly used to treat and process biological tissues used in bioprosthetic heart valve replacements.³¹ Glutaraldehyde fixation, which cross-links collagen fibers in extracellular matrix tissue, is known to increase the bending stiffness of tissues 3–4 fold.³¹ Because the surface tension of residual water caused folding or bending in the thinnest leaflet sections and in the chordal trees, glutaraldehyde fixation was employed to raise the bending stiffness of the tis-

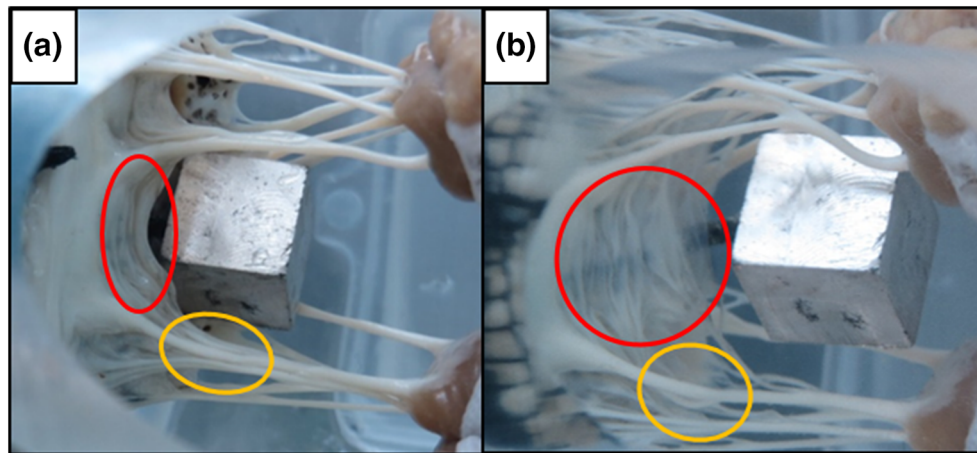


FIGURE 5. The adhesive/cohesive effect of residual water on the MV is shown here. (a) An image of the MV in the CLHS after water has been drained reveals that the thin marginal leaflet tissue folds on itself and the chordal trees bunch together. (b) When the MV is submerged in water, the chordal detail is visible and the anterior leaflet is appreciably larger.

sue enough to significantly reduce folding and bunching, preserving the physiological surface area of the leaflets and detail of the chordal tree. Additionally, it was hypothesized that by fixing the MV tissue as a forward flow was passed over the valve, the effect of diastole on the MV geometry could be captured. This concept has been previously described in recent publications in a more preliminary form, and on a separate cohort of MV samples.²⁸ Significant improvements and modifications to this technique, as well as a more extensive and relevant validation of the technique are described below on a new cohort of five MV samples.

To preserve the diastolic geometry of the MVs for the final microCT imaging step, a vertical fixation loop was designed and assembled, with which glutaraldehyde fixative was run over an MV at a steady flow rate, through a custom nozzle which distributed the flow of fixative evenly over the MV (Fig. 6). With the annulus and PMs in their healthy configuration, the MV was lightly fixed in the vertical configuration for 2 h using 0.5% glutaraldehyde solution. The vertical orientation allows gravity to extend the leaflets normal to the annular plane while the custom nozzle allows even fixation of the leaflet tissue. This creates a more physiological and repeatable mid-diastolic geometry.

After fixation, the CLHS was removed from the fixation loop, and the MV was imaged again by microCT in the three geometric configurations (healthy, IMR, and restrictive annuloplasty), yielding 3D images of each MV in the diastolic state. It is important to note that, though the fixative does stiffen the MV when the annulus and PMs are in their healthy configuration, the tissue remains compliant enough to distort when the annulus and PMs are adjusted to their healthy and diseased configurations. Similarly, bio-prosthetic heart valve replacements are still able to

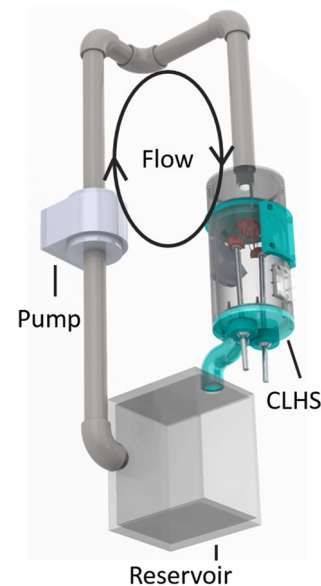


FIGURE 6. A vertical, steady flow loop is used to apply glutaraldehyde fixative. After microCT scans in the loaded condition are taken, the cylindrical left heart simulator (CLHS) is mounted vertically into the loop shown here. The leaflets spread and hang normal to the annular plane as glutaraldehyde solution (0.5% in deionized water) fixes the leaflets in place, yielding a repeatable, anatomical diastolic MV geometry.

open fully under forward flow despite the stiffening induced by glutaraldehyde fixation.

Image Segmentation and Post Processing

Following microCT scanning, images were segmented to create surface meshes of both the fiducial markers and of the MV itself using Avizo segmentation software (FEI, Hillsboro, OR, USA). Centroids of segmented markers were then found, and measure-

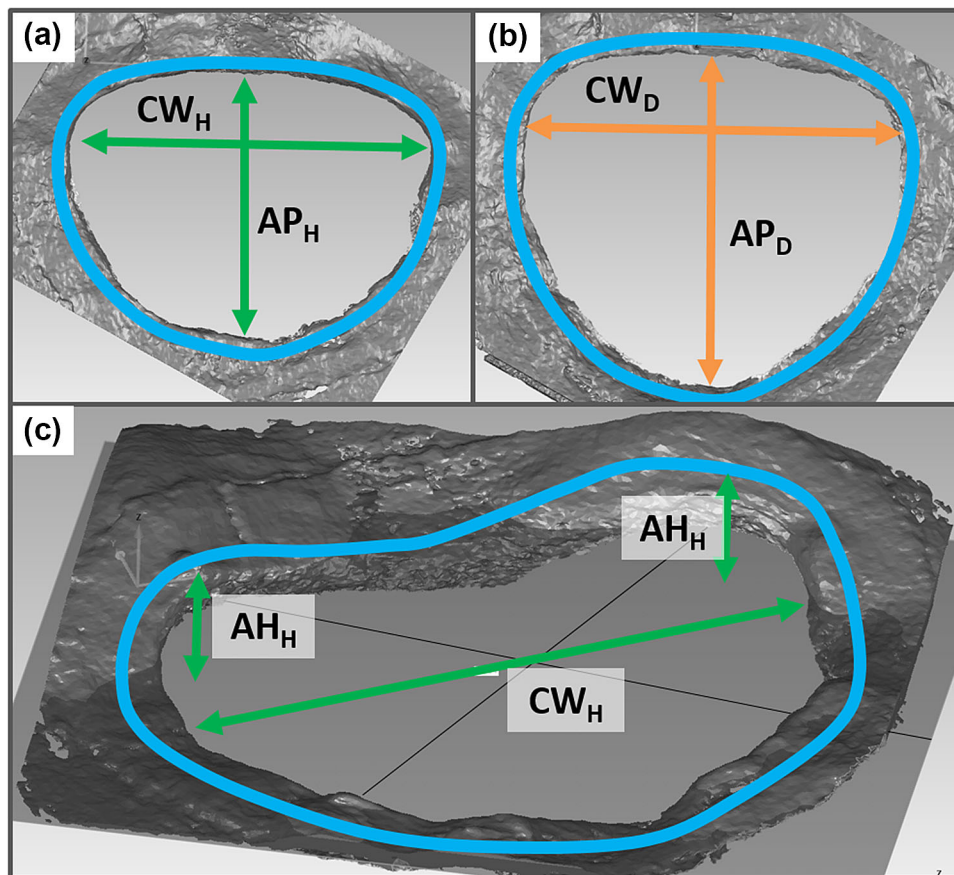


FIGURE 7. Annular measurements of the custom annulus plate are made with microCT images in post-processing. (a) For the healthy geometry, commissural width (CW_H) and anterior–posterior diameter (AP_H) are shown with green arrows while the total annular area (A) is shown within the blue line. (b) The same (CW , AP , A) are shown for the IMR/Diseased annular geometry. (c) The annular height (AH) from plane of the annulus is shown for the healthy geometry. Note that the repaired state simulates a flat annuloplasty ring, and therefore has the same annular areal measurements as the healthy geometry, without the 3D saddle shape.

ments were made on the model leaflets using Geomagic (3D Systems, Rock Hill, SC, USA). Strain calculations were made using the centroids of fiducial markers and a custom MATLAB program (MathWorks, Inc., Natick, MA, USA) following the process described by Rausch *et al.*²² Finally, mitral leaflet dimensional measurements were made on the 3D echo images using Philips QLab software (Philips Healthcare, Andover, MA, USA).

Mitral Annular Geometry Verification Method

To verify the resulting geometric annular changes produced by the custom adjustable annulus plate, the plate was mounted in the CLHS chamber, configured to the healthy geometry and scanned by microCT. The plate was then re-configured to the IMR/diseased geometry and scanned. Since the device was designed to be configured to two discrete annular sizes with either saddle or flat annular profiles, only one scan was performed for each state. The suture cuff of the plate in

both configurations was then segmented. Cartesian coordinates of discrete points following the leaflet hinge line on the suture cuff were then taken. Anterior–posterior diameter (AP), commissural width (CW), and height of the trigones from the annular plane (AH) were all measured as shown in Fig. 7. These dimensions were verified to be in the range of published values from *in vivo* studies.^{5,11,30}

PM Displacement Verification Method

To similarly verify the resulting PM displacements, fiducial markers were applied to the tips of each PM for all five MV samples. In addition to these five samples, the PM manipulation and imaging process was repeated on three additional MV samples, for a total sample size MVs ($n = 8$) used in PM displacement analysis. PMs were moved to the healthy configuration, and the CLHS was scanned by microCT. Next, PMs were displaced to the IMR/diseased configuration, and the CLHS was scanned again by mi-

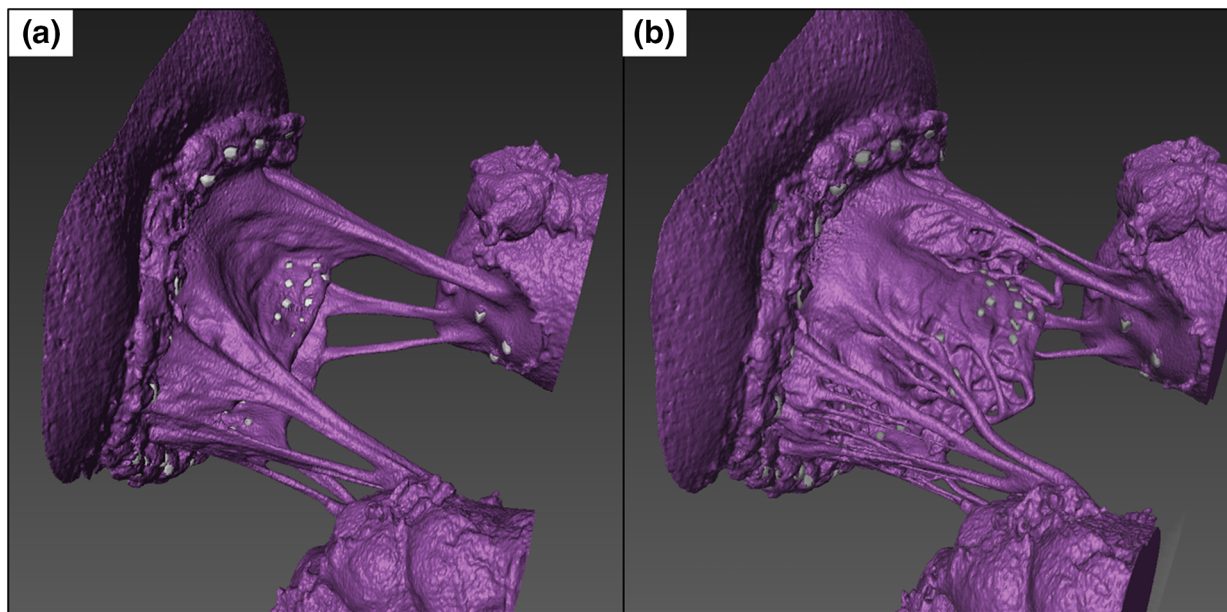


FIGURE 8. Models segmented from microCT images of the same representative MV with- and without fixation. (a) Without fixation, the detail within the folded and bunched structures cannot be distinguished; the leaflet area is under-represented and the chordal trees lack any detail or definition. (b) After glutaraldehyde fixation is performed, the resulting model shows preserved leaflet area and chordal detail. The individual marginal chordae and undulations in the mitral leaflets are captured with high contrast and resolution.

croCT. Markers were segmented, and centroid coordinates were found. Displacement vectors for the posteromedial PM and anterolateral PM were found, and the magnitude of the displacement was compared to those values derived from previously published *in vivo* ovine studies.^{11,25}

MV Fixation Validation Method

To evaluate the use of glutaraldehyde fixation to stiffen the MV and preserve the leaflet dimensions observed under pulsatile flow, a validation trial was performed. In its most refined form, the complete fixation and microCT imaging procedure as presented in this work was performed on five MVs ($n = 5$). Each MV in this trial was first imaged with 3D echo under pulsatile flow. Though the spatial resolution of this imaging modality is inferior to that of microCT, 3D echo is able to capture the coarse geometry of the MV at peak diastole under dynamic flow simulation. This was taken as the ground-truth diastolic MV geometry for the validation of the fixation method. Next, each valve was scanned by microCT in the unloaded state to capture the effect of surface tension on the valve. The MVs were then glutaraldehyde-fixed using the above protocol. Following fixation, the MVs were again imaged by microCT in the unloaded state. Dimensions of the MV leaflets (anterior leaflet area, A1 segment

length, A2 segment length, A3 segment length, and P2 segment length) were measured on the peak diastolic frame of 3D echo and were taken as ground-truth. These measurements were then replicated on both the glutaraldehyde-fixed and unfixed microCT scans, and the measurement difference from ground-truth was found. An acceptable error threshold for all measurements was determined to be $\pm 5\%$ from ground truth.

RESULTS

Diastolic MicroCT Image Detail

Without implementing the glutaraldehyde fixation process, segmented geometries resulting from microCT were appreciably distorted. The leaflets appeared significantly shorter and thicker, and the bunched chordal trees were resolved as large single chordal masses, which appeared to insert only into the margins of the leaflets (Fig. 8a). The segmented geometry of the MV after fixation qualitatively appeared to capture the natural shape and size of the leaflets and substantially more of the chordal tree detail (Fig. 8b). This represents a marked improvement in the quality and consistency of microCT images of excised MVs. Leaflet details and thickness can be seen, in addition to the native chordal tree structure, making an image of this detail valuable for modeling and geometric analysis.

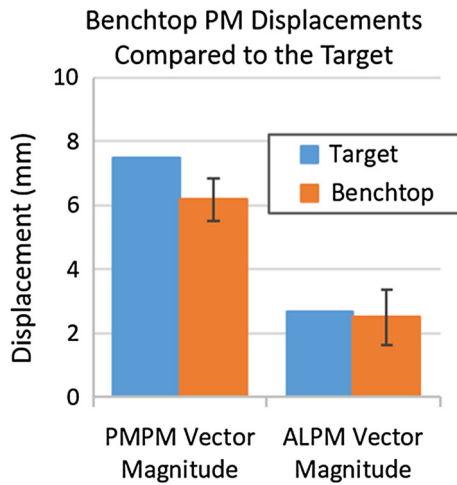


FIGURE 9. Achieved papillary muscle displacement values for the posteromedial and anterolateral papillary muscles (PMPM and ALPM, respectively) measured by microCT compared with target values based on *in vivo* data. Displacements for the PMPM and ALPM were found to be 6.2 ± 1.0 and 2.5 ± 1.3 mm respectively, as compared to values calculated from literature of 7.5 and 2.7 mm, respectively. No significant difference was found between the achieved and desired displacement values for the ALPM ($p = 0.9$). However, that of the PMPM was found to be small, but significant ($p = 0.05$).

Systolic MicroCT and Strain Calculation

Using microCT and fiducial markers (Fig. 4), areal green strain, E^{areal} , on the anterior leaflet was calculated as

$$E^{\text{areal}} = \frac{da - dA}{dA} \quad (1)$$

where da represents the area of a triangular surface element in the systolic configuration, and dA represents that in the diastolic configuration.²⁰ Strain in the belly region was found to be $47.1 \pm 21.5\%$ ($n = 61$ markers). This agrees well with previous *in vitro* studies by Jimenez *et al.* ($36 \pm 14\%$),¹⁵ He *et al.* ($42 \pm 20\%$),¹² and Sacks *et al.* ($47 \pm 10\%$).²⁴ In addition to strain in the belly region, strain in the coaptation zone was calculated. This was found to be $-12.5 \pm 15.8\%$, and presents novel data that cannot be visualized with traditional stereo-photogrammetry techniques due to the lack of optical access. Finally, the detail of the MV leaflets and chordal structure can be fully appreciated in the systolic state (Fig. 4).

PM Displacement Verification

Displacements for the posteromedial PM and anterolateral PM were found to be 6.2 ± 1.0 and 2.5 ± 1.3 mm respectively, as compared to values target values based on *in vivo* studies of 7.5 and 2.7 mm,²⁵ respectively (Fig. 9). Difference in dis-

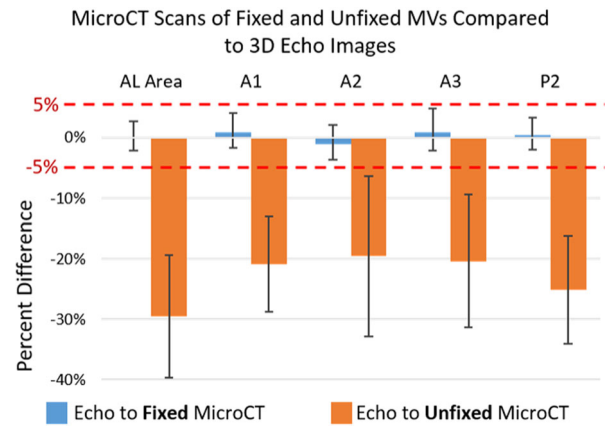


FIGURE 10. MicroCT scans of each MV ($n = 5$) in the diastolic state with- and without glutaraldehyde fixation are compared to the peak diastolic frame of 3D echo for the same MVs under pulsatile flow. Mean and 95% confidence interval are shown for the differences observed in identical measurements made on the diastolic microCT scan and on a mid-diastolic frame of 3D echo images. Anterior leaflet lengths (A1–A3), posterior leaflet length (P2) and anterior leaflet area (Area) were all found to be equivalent to within $\pm 5\%$ with 95% confidence between the glutaraldehyde fixed images and the dynamic 3D echo images ($p < 0.05$). Percent change of the above measurements from the 3D echo images to the unfixed microCT images was found to be significantly negative ($p < 0.001$), revealing substantial MV shrinkage in the range of 20–30% when imaging without fixation.

placement of the posteromedial PM was not found to be significant ($p = 0.9$). Though the anterolateral PM displacement value was significantly under-represented ($p = 0.05$), the difference was just 1.3 mm.

Diastolic CT Geometry Validation

Finally, microCT and 3D echo were used to validate the fixation procedure for obtaining a physiologically accurate diastolic MV geometry. Summarized in Fig. 10, all leaflet length and area measurements from the glutaraldehyde-fixed microCT scan were found to be equivalent within $\pm 5\%$ to those measurements made on the peak diastolic frame of 3D echo (95% confidence). Without fixation, all length and area measurements were found to be significantly smaller than both 3D echo derived measurements and measurements from fixed microCT scans ($p < 0.005$). Furthermore, the standard deviations of these measurements were appreciably smaller after fixation, indicating not only improved accuracy and detail, but also improved consistency over previous methods.²⁸

DISCUSSION

Computational models which aim to capture MV structure and function across states of health, disease,

and repair require comprehensive data sets to construct the finite element mesh, provide boundary conditions, and to validate model performance in all cases. To this end, we have detailed *ex vivo* hardware and methodologies which allow for repeated-measures data collection wherein all geometric changes can be performed on a single MV, and the valve can be imaged with microCT in each state. Additionally, models that seek to capture finer detail in the leaflets and subvalvular apparatus require high-resolution imaging, and specimen preparation techniques. We have also detailed the specific microCT imaging techniques used to reliably and repeatably prepare the valve to simulate the diastolic state, and to load the valve simulating systole.

The annular geometries created by the adjustable annulus plate were verified in the range of published values,^{5,30} and the PMs were repeatably displaced to mimic LV remodeling. The unprecedented ability to quickly perform these geometric changes between microCT image acquisitions on a single MV has provided a comprehensive package of image data for the construction and validation of MV computational models. This study was limited to specific diseased and repaired geometries (IMR and restrictive flat annuloplasty), however, the modularity of the CLHS can be leveraged to extend the experimental work to many different types of functional disease and repair. We have reproduced symmetric annular geometries, but the annular segments are individually adjustable, thus enabling future experiments to examine the effect of non-uniform annular dilatation on MV function. Furthermore, novel equipment to reproduce additional geometries can be designed and implemented within the existing chamber and data collection platform. For example, a Kron repair with saddle annuloplasty could be simulated and imaged.

Previously published modeling work speaks to the importance of representing chordal branching, leaflet thickness, and subject-specific structures to finite element simulation of MV function.^{19,28,33} Models using an unverified, idealized or misrepresented MV structure can lead to an inaccurate simulation and result in erroneous conclusions.³² The method of glutaraldehyde treatment presented herein showed an improved ability to preserve MV leaflet surface area during diastolic imaging, as compared to mid-diastolic 3D echo images. Other concepts were also tested, but were not successful. These included testing additives to reduce the surface tension of the residual water on the valve, but the water content of the valve and the effect of gravity continued to cause significant distortion. Glutaraldehyde fixation was determined to be the most efficacious method of preserving MV leaflet surface area and detail. Furthermore, the vertical flow orientation

was adopted, along with a custom atrial nozzle in order to orient the valve with the leaflets hanging vertically and distribute the flow of glutaraldehyde over the tissue. This represents significant advancements over first iteration, where a horizontal loop orientation was used, and the leaflet areas were not yet equivalent to the reference state.²⁸

The glutaraldehyde fixation technique also qualitatively preserved more detail in the subject-specific chordal tree (Fig. 8b). When compared to images of the MV without fixation, the fixed geometries are not only significantly closer to ground truth 3D echo images; the variability of the differences is also much smaller. The 95% confidence interval windows of the “3D echo to unfixed microCT” comparison are appreciably larger than those of the “3D echo to fixed microCT” comparison in Fig. 10. This indicates that the effect of surface tension on the valve is more random, and can vary widely from valve to valve, while fixation substantially mitigates that variability and introduces repeatability to microCT scans.

For the validation of MV model performance, we have also developed techniques to provide microCT images of the same MV samples loaded at different pressures (30 and 100 mmHg). This combined with the addition of a grid of fiducial markers allows discrete one-to-one tracking of the MV leaflets, annulus, chordae and papillary muscles across the different geometric configurations and states of loading (shown in healthy state in Fig. 4). After creating a MV geometry from the diastolic microCT scans provided, the grid may be used to manipulate the model and map microstructural tissue data to the model. Following the finite element simulation of MV closure, the accuracy of the systolic MV geometry can be directly compared to the experimental results using discrete marker positions from the microCT scans. Additionally, the fiducial markers can be used to measure directional strain in response to both levels of loading,²⁰ and fine-tune the material properties of the FE model.

Thus far, these *ex vivo* developments have enabled the geometric characterization of the MV leaflets and chordae tendineae to an unprecedented level of detail,¹⁶ and work is ongoing to create and validate high-fidelity biomechanical models of the MV which link healthy, diseased and surgically repaired conditions.^{16,19} *In vivo* imaging has long been the primary source of image data for computational models of the valves of the heart.²⁶ However, certain limitations of clinical imaging exist, such as low spatial resolution and uncontrollable factors. These limitations may be surmountable with the addition of *ex vivo* imaging and simulation. Looking forward, the detailed geometric analyses and MV models enabled by this work may be used to augment *in vivo* and clinical inputs, leading to

high-fidelity modeling and repair planning at the point-of-care.¹⁶

Limitations

A few key limitations of the platform must be considered. First, previous work has reported the limited magnitudes of PM geometric perturbations possible *ex vivo*.²⁵ Without the capacity for active tissue remodeling that exists *in vivo*,²³ acute *ex vivo* displacement of PMs to those magnitudes seen *in vivo* risks tissue tearing. Therefore, intermediary displacement targets were selected based on *in vivo* data.^{10,25,27} Work is ongoing to improve the accuracy of PM displacement by eliminating the bulk of the PM tissue in the mounting system and preserving only the chordal insertion points on the PM.

Additionally, the mitral annulus and PMs remained static during microCT imaging. Recent modeling work has also spoken to the importance of capturing the dynamic motion of these structures in modeling,³² and changes in LV and annular motion may have an impact on valve performance in certain functional MR pathologies. In IMR due to inferior MI, dynamic motion may affect the valve performance, but the primary effect has been attributed to PM displacement and annular dilatation.³⁰ Previous publications have shown that the MV systolic geometry observed *in vivo* in healthy and chronic IMR ovine subjects can be replicated *in vitro* in left heart simulators without dynamic motion of the PMs and annulus.²⁵ Due to the limitation of static microCT imaging, we have designed the platform to simulate the healthy, diseased and repaired geometries in a static manner. To overcome this limitation in future studies, the best practice may be the piece-wise augmentation of these models with *in vivo* dynamic displacement data to incorporate PM and annular motion into computational models.

ACKNOWLEDGMENTS

This work was partially supported by the National Science Foundation Graduate Research Fellowship (ELP) under Grant DGE-1148903, as well as by the National Heart, Lung, and Blood Institute under Grant R01HL119297.

CONFLICT OF INTEREST

No benefits in any form have been received from a commercial party related directly or indirectly to the subject of this manuscript.

REFERENCES

- ¹Acker M. A., M. K. Parides, L. P. Perrault, A. J. Moskowitz, A. C. Gelijns, P. Voisine, P. K. Smith, J. W. Hung, E. H. Blackstone, J. D. Puskas, M. Argenziano, J. S. Gammie, M. Mack, D. D. Ascheim, E. Bagiella, E. G. Moquete, T. B. Ferguson, K. A. Horvath, N. L. Geller, M. A. Miller, Y. J. Woo, D. A. D'Alessandro, G. Ailawadi, F. Dagenais, T. J. Gardner, P. T. O'Gara, R. E. Michler, I. L. Kron, and CTSN. Mitral-valve repair versus replacement for severe ischemic mitral regurgitation. *N. Engl. J. Med.* 370: 23–32, 2014.
- ²Borger, M. A., A. Alam, P. M. Murphy, T. Doenst, and T. E. David. Chronic ischemic mitral regurgitation: repair, replace or rethink? *Ann. Thorac. Surg.* 81:1153–1161, 2006.
- ³Braunberger, E., A. Deloche, A. Berrebi, F. Abdallah, J. A. Celestin, P. Meimoun, G. Chatellier, S. Chauvaud, J. N. Fabiani, and A. Carpentier. Very long-term results (more than 20 years) of valve repair with Carpentier's techniques in nonrheumatic mitral valve insufficiency. *Circulation* 104:18–111, 2001.
- ⁴Carpentier, A., D. H. Adams, and F. Filsofi. *Carpentier's Reconstructive Valve Surgery*. Philadelphia, PA: Elsevier Health Sciences, 2011.
- ⁵Daimon, M., G. Saracino, S. Fukuda, Y. Koyama, J. Kwan, J. M. Song, D. A. Agler, A. M. Gillinov, J. D. Thomas, and T. Shiota. Dynamic change of mitral annular geometry and motion in ischemic mitral regurgitation assessed by a computerized 3D echo method. *Echocardiography* 27:1069–1077, 2010.
- ⁶De Bonis, M., D. Ferrara, M. Taramasso, M. C. Calabrese, A. Verzini, N. Buzzatti, and O. Alfieri. Mitral replacement or repair for functional mitral regurgitation in dilated and ischemic cardiomyopathy: is it really the same? *Ann. Thorac. Surg.* 94:44–51, 2012.
- ⁷Einstein, D. R., F. Del Pin, X. Jiao, A. P. Kuprat, J. P. Carson, K. S. Kunzelman, R. P. Cochran, J. M. Guccione, and M. B. Ratcliffe. Fluid–structure interactions of the mitral valve and left heart: comprehensive strategies, past, present and future. *Int. J. Numer Methods Eng.* 26:348–380, 2010.
- ⁸Fedak, P. W., P. M. McCarthy, and R. O. Bonow. Evolving concepts and technologies in mitral valve repair. *Circulation* 117:963–974, 2008.
- ⁹Gillinov, A. M., P. N. Wierup, E. H. Blackstone, E. S. Bishay, D. M. Cosgrove, J. White, B. W. Lytle, and P. M. McCarthy. Is repair preferable to replacement for ischemic mitral regurgitation? *J. Thorac. Cardiovasc. Surg.* 122:1125–1141, 2001.
- ¹⁰Gorman III, J. H., R. C. Gorman, B. M. Jackson, Y. Enomoto, M. G. St John-Sutton and L. H. Edmunds, Jr. Annuloplasty ring selection for chronic ischemic mitral regurgitation: lessons from the ovine model. *Ann. Thorac. Surg.* 76: 1556–1563, 2003.
- ¹¹Gorman, J. H., B. M. Jackson, Y. Enomoto, and R. C. Gorman. The effect of regional ischemia on mitral valve annular saddle shape. *Ann. Thorac. Surg.* 77:544–548, 2004.
- ¹²He, Z., M. S. Sacks, L. Baijens, S. Wanant, P. Shah, and A. P. Yoganathan. Effects of papillary muscle position on *in vitro* dynamic strain on the porcine mitral valve. *J. Heart Valve Dis.* 12:488–494, 2003.
- ¹³Hung, J., L. Papakostas, S. A. Tahta, B. G. Hardy, B. A. Bollen, C. M. Duran, and R. A. Levine. Mechanism of recurrent ischemic mitral regurgitation after annuloplasty:

- continued LV remodeling as a moving target. *Circulation* 110:II85–II90, 2004.
- ¹⁴Jung, B., and A. Vahanian. Epidemiology of acquired valvular heart disease. *Can. J. Cardiol.* 30:962–970, 2014.
- ¹⁵Jimenez, J. H., S. W. Liou, M. Padala, Z. He, M. Sacks, R. C. Gorman, J. H. Gorman, 3rd, and A. P. Yoganathan. A saddle-shaped annulus reduces systolic strain on the central region of the mitral valve anterior leaflet. *J. Thorac. Cardiovasc. Surg.* 134:1562–1568, 2007.
- ¹⁶Khalighi, A. H., A. Drach, F. M. ter Huurne, C. H. Lee, C. Bloodworth, E. L. Pierce, M. O. Jensen, A. P. Yoganathan, and M. S. Sacks. A comprehensive framework for the characterization of the complete mitral valve geometry for the development of a population-averaged model. *Funct. Imaging Model. Heart (FIMH 2015)* 9126:164–171, 2015.
- ¹⁷Kunzelman, K., M. S. Reimink, E. D. Verrier and R. P. Cochran. Replacement of mitral valve posterior chordae tendinae with expanded polytetrafluoroethylene suture: a finite element study. *J. Card. Surg.* 11: 136–145; discussion 146, 1996.
- ¹⁸Kuwahara, E., Y. Otsuji, Y. Iguro, T. Ueno, F. Zhu, N. Mizukami, K. Kubota, K. Nakashiki, T. Yuasa, B. Yu, T. Uemura, K. Takasaki, M. Miyata, S. Hamasaki, A. Kisanuki, R. A. Levine, R. Sakata, and C. Tei. Mechanism of recurrent/persistent ischemic/functional mitral regurgitation in the chronic phase after surgical annuloplasty: importance of augmented posterior leaflet tethering. *Circulation* 114:1529–1534, 2006.
- ¹⁹Lee, C. H., P. J. A. Oomen, J. P. Rabbah, A. Yoganathan, R. C. Gorman, J. H. Gorman, R. Amini, and M. S. Sacks. A high-fidelity and micro-anatomically accurate 3D finite element model for simulations of functional mitral valve. *Funct. Imaging Model. Heart* 7945:416–424, 2013.
- ²⁰Pierce, E. L., C. H. Bloodworth, IV, A. Naran, T. F. Easley, M. O. Jensen, and A. P. Yoganathan. Novel method to track soft tissue deformation by micro-computed tomography: application to the mitral valve. *Ann. Biomed. Eng.* 44(7):2273–2281, 2015.
- ²¹Rabbah, J.-P., N. Saikrishnan, and A. P. Yoganathan. A novel left heart simulator for the multi-modality characterization of native mitral valve geometry and fluid mechanics. *Ann. Biomed. Eng.* 41:305–315, 2013.
- ²²Rausch, M. K., W. Bothe, J. P. Kvitting, S. Goktepe, D. C. Miller, and E. Kuhl. In vivo dynamic strains of the ovine anterior mitral valve leaflet. *J. Biomech.* 44:1149–1157, 2011.
- ²³Rausch, M. K., F. A. Tibayan, D. C. Miller, and E. Kuhl. Evidence of adaptive mitral leaflet growth. *J. Mech. Behav. Biomed. Mater.* 15:208–217, 2012.
- ²⁴Sacks, M. S., Z. He, L. Baijens, S. Wanant, P. Shah, H. Sugimoto, and A. P. Yoganathan. Surface strains in the anterior leaflet of the functioning mitral valve. *Ann. Biomed. Eng.* 30:1281–1290, 2002.
- ²⁵Siefert, A. W., J. P. Rabbah, K. J. Koomalsingh, S. A. Touchton, Jr, N. Saikrishnan, J. R. McGarvey, R. C. Gorman, J. H. Gorman, III, and A. P. Yoganathan. In vitro mitral valve simulator mimics systolic valvular function of chronic ischemic mitral regurgitation ovine model. *Ann. Thorac. Surg.* 95:825–830, 2013.
- ²⁶Sun, W., C. Martin, and T. Pham. Computational modeling of cardiac valve function and intervention. *Annu. Rev. Biomed. Eng.* 16:53–76, 2014.
- ²⁷Tibayan, F. A., F. Rodriguez, M. K. Zasio, L. Bailey, D. Liang, G. T. Daughters, F. Langer, N. B. Ingels, Jr. and D. C. Miller. Geometric distortions of the mitral valvular-ventricular complex in chronic ischemic mitral regurgitation. *Circulation* 108(Suppl 1): II116–II121, 2003.
- ²⁸Toma, M., C. H. Bloodworth, IV, D. R. Einstein, E. L. Pierce, R. P. Cochran, A. P. Yoganathan, and K. S. Kunzelman. High-resolution subject-specific mitral valve imaging and modeling: experimental and computational methods. *Biomech. Model. Mechanobiol.* 2016. doi: 10.1007/s10237-016-0786-1.
- ²⁹Toma, M., M. O. Jensen, D. R. Einstein, A. P. Yoganathan, R. P. Cochran, and K. S. Kunzelman. Fluid-structure interaction analysis of papillary muscle forces using a comprehensive mitral valve model with 3D chordal structure. *Ann. Biomed. Eng.* 44(4):942–953, 2015.
- ³⁰Vergnat, M., A. S. Jassar, B. M. Jackson, L. P. Ryan, T. J. Eperjesi, A. M. Pouch, S. J. Weiss, A. T. Cheung, M. A. Acker, J. H. Gorman, and R. C. Gorman. Ischemic mitral regurgitation: a quantitative three-dimensional echocardiographic analysis. *Ann. Thorac. Surg.* 91:157–164, 2011.
- ³¹Vesely, I., and D. Boughner. Analysis of the bending behaviour of porcine xenograft leaflets and of natural aortic valve material: bending stiffness, neutral axis and shear measurements. *J. Biomech.* 22:655–671, 1989.
- ³²Votta, E., E. Caiani, F. Veronesi, M. Soncini, F. M. Montevecchi, and A. Redaelli. Mitral valve finite-element modelling from ultrasound data: a pilot study for a new approach to understand mitral function and clinical scenarios. *Philos. Trans. A Math. Phys. Eng. Sci.* 366:3411–3434, 2008.
- ³³Votta, E., T. B. Le, M. Stevanella, L. Fusini, E. G. Caiani, A. Redaelli, and F. Sotiropoulos. Toward patient-specific simulations of cardiac valves: state-of-the-art and future directions. *J. Biomech.* 46:217–228, 2013.
- ³⁴Votta, E., F. Maisano, M. Soncini, A. Redaelli, F. M. Montevecchi, and O. Alfieri. 3-D computational analysis of the stress distribution on the leaflets after edge-to-edge repair of mitral regurgitation. *J. Heart Valve Dis.* 11:810–822, 2002.
- ³⁵Wang, Q., and W. Sun. Finite element modeling of mitral valve dynamic deformation using patient-specific multislices computed tomography scans. *Ann. Biomed. Eng.* 41:142–153, 2013.
- ³⁶Yoganathan, A. P., W. H. Corcoran, and E. C. Harrison. Pressure drops across prosthetic aortic heart valves under steady and pulsatile flow—in vitro measurements. *J. Biomech.* 12:153–164, 1979.